SANDIA REPORT SAND82-8201 • Unlimited Release
Printed January 1982

Slow Strain Rate Testing of Alloy 800 in Molten Nitrate Salts

S. H. Goods

Prepared by
Sandia National Laboratories
Albuquerque, New Mexico 87185 and Livermore, California 94550
for the United States Department of Energy
under Contract DE-AC04-76DP00789

SF2900Q(8-81)

Issued by Sandia Laboratories, operated for the United States Department of Energy by Sandia Corporation.

NOTICE

SAND82-8201
Unlimited Release
Printed January 1982

SLOW STRAIN RATE TESTING OF ALLOY 800 IN MOLTEN NITRATE SALTS

S. H. Goods
Materials Science Division
Sandia National Laboratories, Livermore

ABSTRACT

An experimental technique has been developed to examine the interaction between deformation and the exposure of certain high temperature structural alloys to oxidizing molten salt environments. The experimental program involved performing a series of long-term tensile tests over a wide range of strain rates. Fracture strain reduction in area and ultimate strength (UTS) were monitored as parameters indicative of an alloy's susceptibility to enviornmental degradation.

For Incoloy Alloy 800 tested at 600°C in the salt medium and at initial strain rates between 2×10^{-7} sec^{-1} and 1×10^{-5} sec^{-1} no appreciable loss of ductility, as measured by reduction in area, was observed relative to control specimens tested in air at the same temperature and strain rates. Similarly, fracture strain and UTS were essentially unaffected by exposure to the oxidizing environment.

The structure of the oxide film formed by contact of the specimens to the molten salt was affected by the imposed continuous deformation. Deformation resulted in an oxide which was thicker than that formed on undeformed salt-exposed surfaces. While this difference in oxide thickness was a measurable phenomenon, the increased rate of oxidation was not great enough to appreciably alter alloy mechanical behavior in the salt compared to that measured in air. In addition, fine subsurface cracks were observed in those oxides formed on deformed surfaces.

ACKNOWLEDGEMENT

The author wishes to acknowledge the assistance of T. J. Sage in the design, construction and operation of the SSRT equipment.

TABLE OF CONTENTS

ILLUSTRATIONS

INTRODUCTION

Advanced designs of Solar Central Receivers (SCR) call for the use of a condensed phase fluid as the coolant or heat transfer medium. The choice of that fluid is largely one of economics based upon a combination of factors including its costs and optimal thermophysical characteristics (1,2). For current receiver designs, the choice of this fluid has been narrowed to the nitrate based salts. These mixtures of sodium nitrate and potassium nitrate have melting points which vary between 200°C and 350°C depending upon their specific composition and have been used for some time in a variety of industrial applications including both process heat and heat treating operations. The major concern regarding their use in SCR applications has been the relative lack of information concerning their intrinsic thermochemical and thermophysical properties and stability at temperatures above those of normal industrial experience. Additional concerns involve their influence on the long-term behavior of containment materials at the elevated temperatures representative of receiver panel operating conditions (peak temperatures near 600°C).

While the stability and thermophysical properties of these salts have been addressed elsewhere (3-5), this report details the results of an experimental program in which the effects of long-term salt exposure on the mechanical properties of Incoloy Alloy 800 have been evaluated. This austenitic stainless steel was chosen as it represents the most likely material to be used in the fabrication of the receiver tube panel array. Because of its high alloy content, it has superior strength to that of 316SS or 304SS at the anticipated maximum operating temperatures.

APPLICABILITY OF THE SLOW STRAIN RATE TEST TO SCR ENVIRONMENTS

During sunlight hours, complex thermal strains will develop in receiver tube panels due to their one-sided heating by redirected sunlight. Diurnal cycling as well as intermittent cloud cover will induce in the receiver tubes a high strain amplitude thermal fatigue cycle with long hold periods at maximum temperatures. At peak stress levels, the temperatures will be well into the creep regime of I800. While the effects of the resulting plastic relaxation processes and creep-fatigue interaction on bulk mechanical properties must eventually be considered, the present work deals with the combined effects of molten salt induced surface attack and continuous monotonic deformation; the effects are studies through a series of slow strain rate tensile tests (SSRT).

Previous work utilizing the SSRT technique has been confined largely to the study of stress corrosion cracking and hydrogen embrittlement in aqueous media (6). However, the technique is valid for the study of material compatibility in molten salt environments as well. Earlier studies have shown that both the austenitic and ferritic stainless steels suffer a uniform surface attack when immersed in these nitrate salts for extended periods of time (7,8) in the absence of deformation. It is necessary therefore to perform the mechanical testing at rates slow enough to allow the test alloy to interact with the corrosive environment.

The slow strain rate test consists of the application of a constant extension rate imposed on a smooth tensile specimen which in turn is exposed to the environment of interest. Because of the somewhat arbitrary test conditions, the results are usually compared to the results of tests performed on specimens exposed to an inert or reference environment (in the present case, air) under identical conditions of strain rate and temperature. Typically, reduction in area (RA), strain to fracture and ultimate tensile strength (UTS) are measured as parameters which determine the susceptibility of an alloy to environmental degradation. The test is thus a versatile method for both the detection of the presence of an environmental or stress corrosion cracking phenomenon as well as for the analysis of the critical variables which may contribute to the observed material degradation. The variables which may be screened include the test or environmental exposure temperature, the particular nitrate salt chemistry or impurity content as well as the metallurgical condition of the alloy under investigation.

Strain rate is a critical variable in the detection of a localized cracking phenomenon in a material which undergoes uniform surface attack in an aggressive medium. Figure 1 schematically illustrates the expected strain rate dependence of a material which suffers from an environmentally induced loss of ductility. In Region I the strain rate is so rapid and the resulting test time is so short that a specimen can deform and fracture before it can interact with the environment. Failure therefore occurs in a normal ductile mode. In Region II environmentally induced embrittlement occurs and the loss of ductility can be due to any of several factors. The continuous deformation results in a porous or cracked oxide scale and thus allows for an increased rate of corrosion. The concomitant loss of load bearing cross-sectional area may result in the earlier onset of necking and fracture. Alternatively, the buildup of residual stresses within the surface scale as it forms can, when coupled to the imposed deformation, allow the oxide to scale or flake off the specimen surface and expose fresh base metal. This would also tend to increase the overall rate of scale formation and increase the rate of metal loss. Finally, deformation-induced cracking of near surface grain boundaries can allow the aggressive environment to penetrate to regions deep within the specimen thereby leading to earlier fracture.

EXPERIMENTAL PROCEDURE

Tensile tests were performed on Incoloy Alloy 800 (heat no. HH8579) bar stock supplied by Huntington Alloys. The alloy was tested in the mill annealed condition and had the composition given in Table 1 below. Sheet tensile specimens were machined from the stock using EDM techniques and had

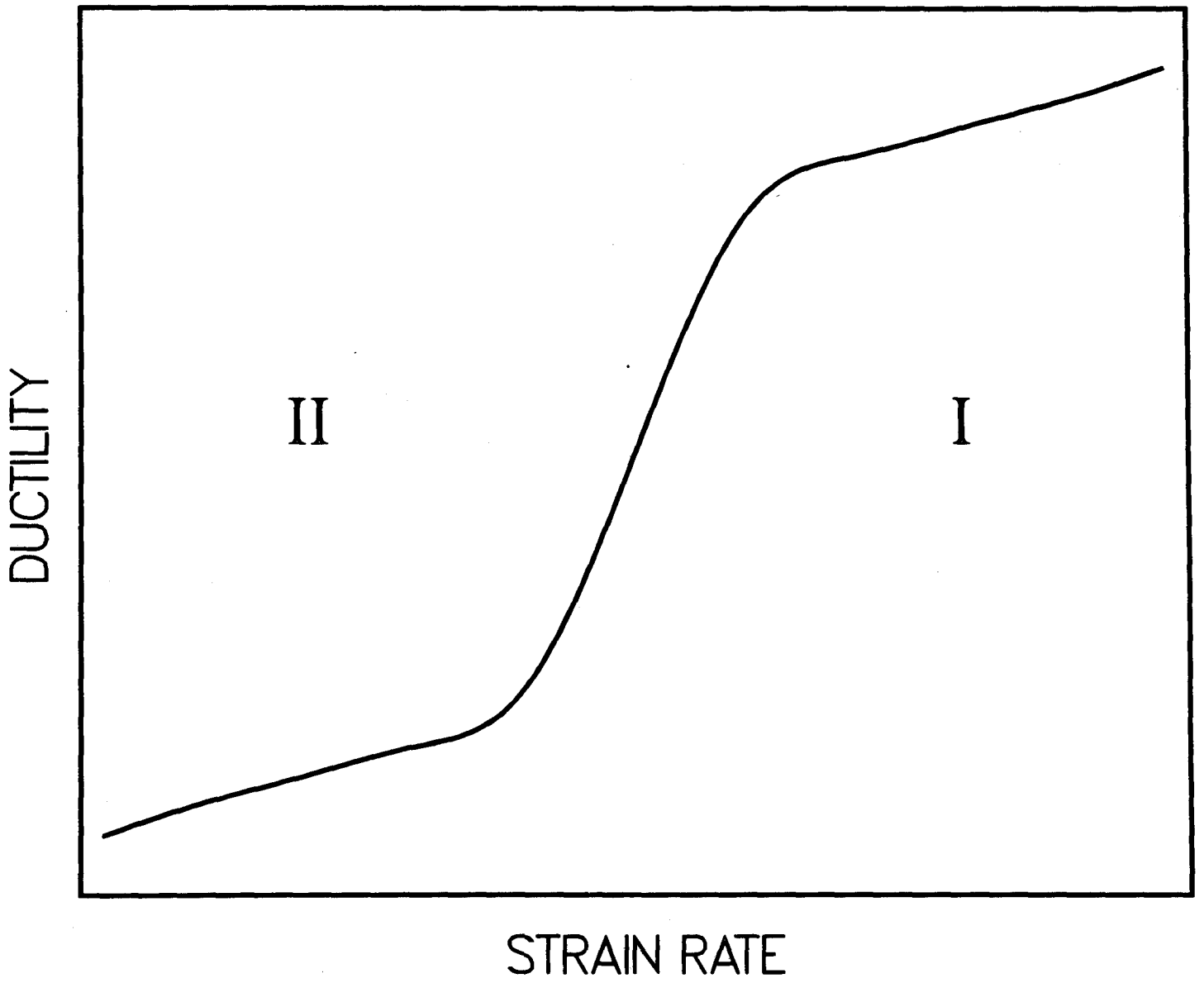

Figure 1. Schematic representation of the effect of strain rate on material ductility as measured in a SSRT experiment for a material which suffers from an environmentally induced embrittlement

TABLE 1

Incoloy Alloy 800 Composition (wt. pct.)

Cr	Ni	Fe	C	Ti	Al	Si	Ni	Mn
19.8	32.9	44.6	0.08	0.47	0.42	0.12	0.02	N.A.

reduced gage sections with 1.27mm x 6.35mm cross-section. In order to test for the effect of surface finish on oxidation characteristics, one side of the specimen was ground and polished to a 600 grit finish on silicon carbide papers prior to immersion in the salt and mechanical testing.

The slow strain rate test facility shown in Figure 2 consisted of two identical load frames each with an 18 kN maximum load rating. The frames are geared to allow uniform extension rates of from 2.54×10^{-8} mm/sec to 2.54×10^{-4} mm/sec. Initial strain rates were computed on the basis of the specimen gage length and the chosen extension rate. Specimens were fixtured in the rigid 4 column cage suspended below the upper cross-head. The furnace body was then raised up around the specimen. To contain the molten salt, a 316SS salt pot with a water cooled collar was placed in the furnace cavity. The particular salt composition used was a 60 wt. % $NaNO_3$ -40 wt.% KNO_3 mixture. The water cooling was necessary to contain the salt within the container at the high test temperature (7). Temperature was controlled and monitored via type K thermocouples positioned along the specimen gage length. Using a Eurotherm temperature controller and power supply, temperature could be maintained to within $\pm$ 0.5°C of set point. The furnace was a Lindberg 203mm diameter crucible furnace. Load vs time data was recorded continuously on a low speed Honeywell strip-chart recorder.

Scanning electron microscopy (SEM) was used to observe fracture surfaces on both the air and salt exposed specimens. Oxide structures were observed using both SEM and optical microscopy.

RESULTS AND DISCUSSION

Figure 3 shows the stress-strain curves generated for Alloy 800 tested in air at 600°C and at the strain rates indicated. While the ultimate strength of this alloy was clearly strongly rate dependent, the engineering fracture strain was only very weakly so. The gradual and continuous unloading of the specimen after UTS at the test temperature reflects the great resistance of the alloy to localized necking at these low strain rates. Even at very large strains deformation remained uniform and fracture occured as the result of extensive grain boundary cracking rather than being due to the onset of plastic instability.

Figure 4 shows the stress-strain curves generated for Alloy 800 tested in salt at 600°C and at the same strain rates as in the previous figure. Thus for tests done at the same strain rate, total test time and therefore total salt exposure times were roughly equivalent, varying from nearly 1000 hours for the slowest tests to less than 24 hours for the test run at the fastest initial strain rates. The tensile curves for all specimens tested in salt exhibited the same characteristic shape as those tested in air.

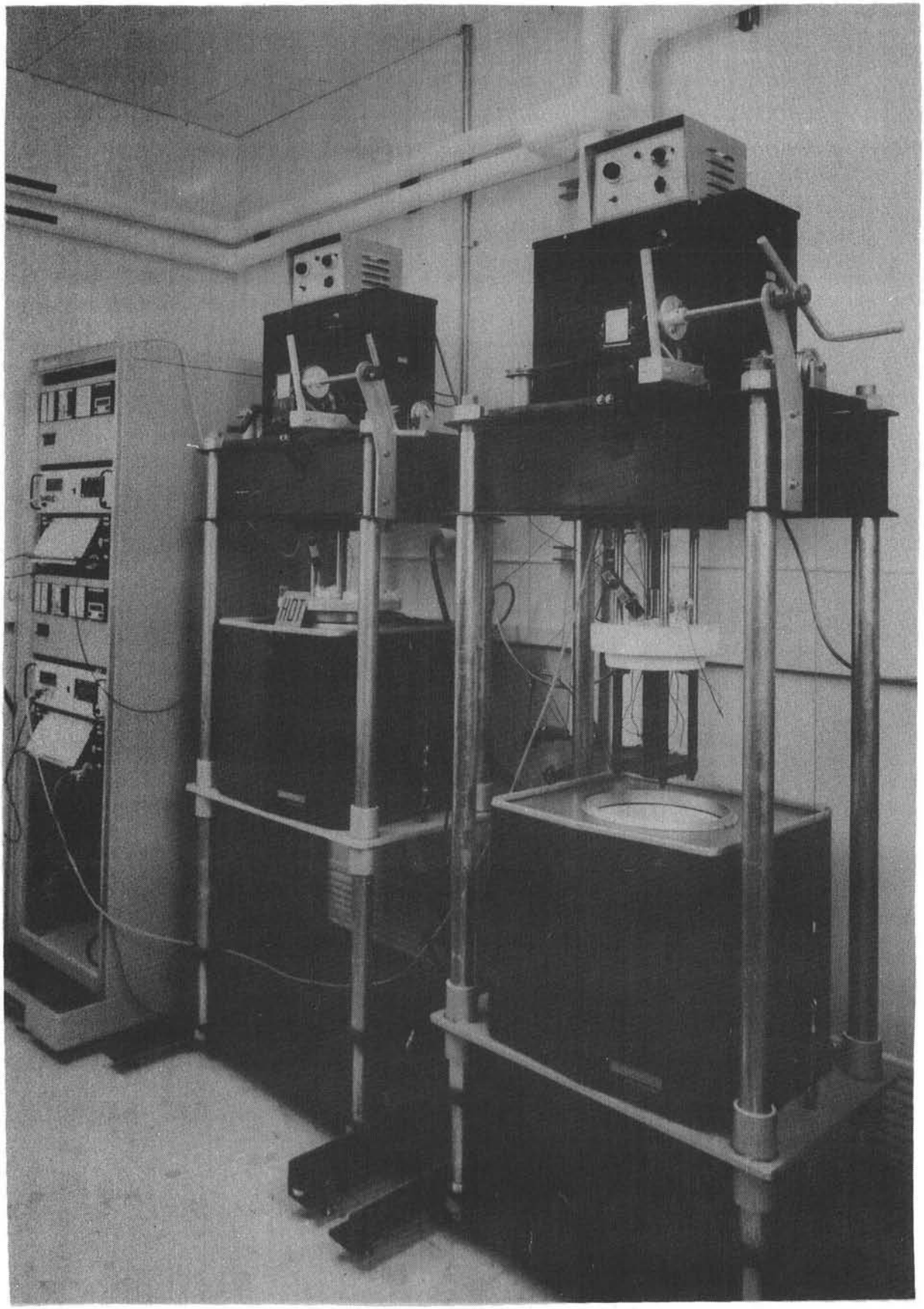

Figure 2. The SSRT facility consists of two identical load frames each with an 18 kN maximum load rating. Load vs. time data is acquired on low speed strip chart recorders.

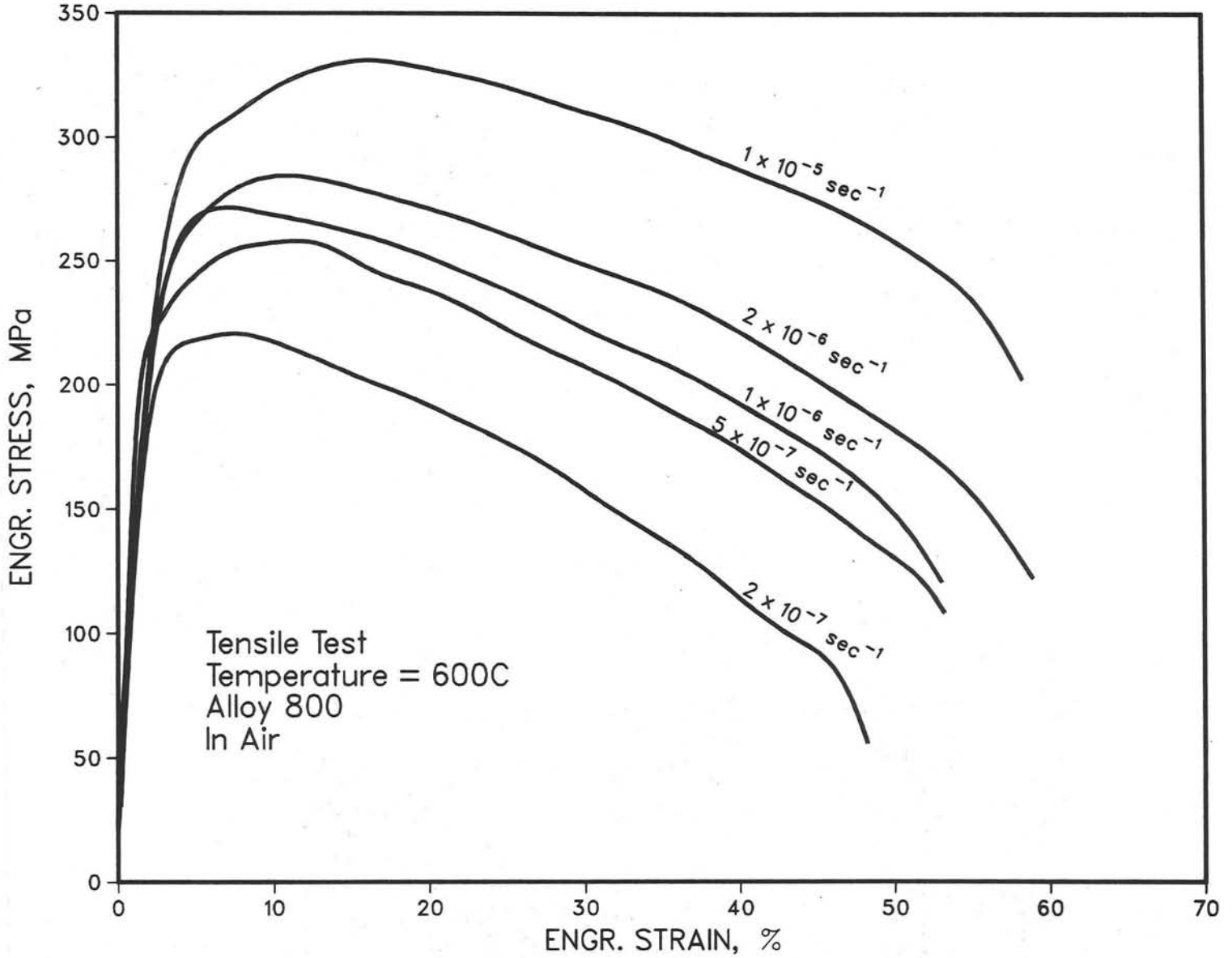

Figure 3. Stress-strain curves for Alloy 800 tested at 600°C in air at the strain rates indicated. Deformation at high strains remains uniform with little tendency for localized necking to occur.

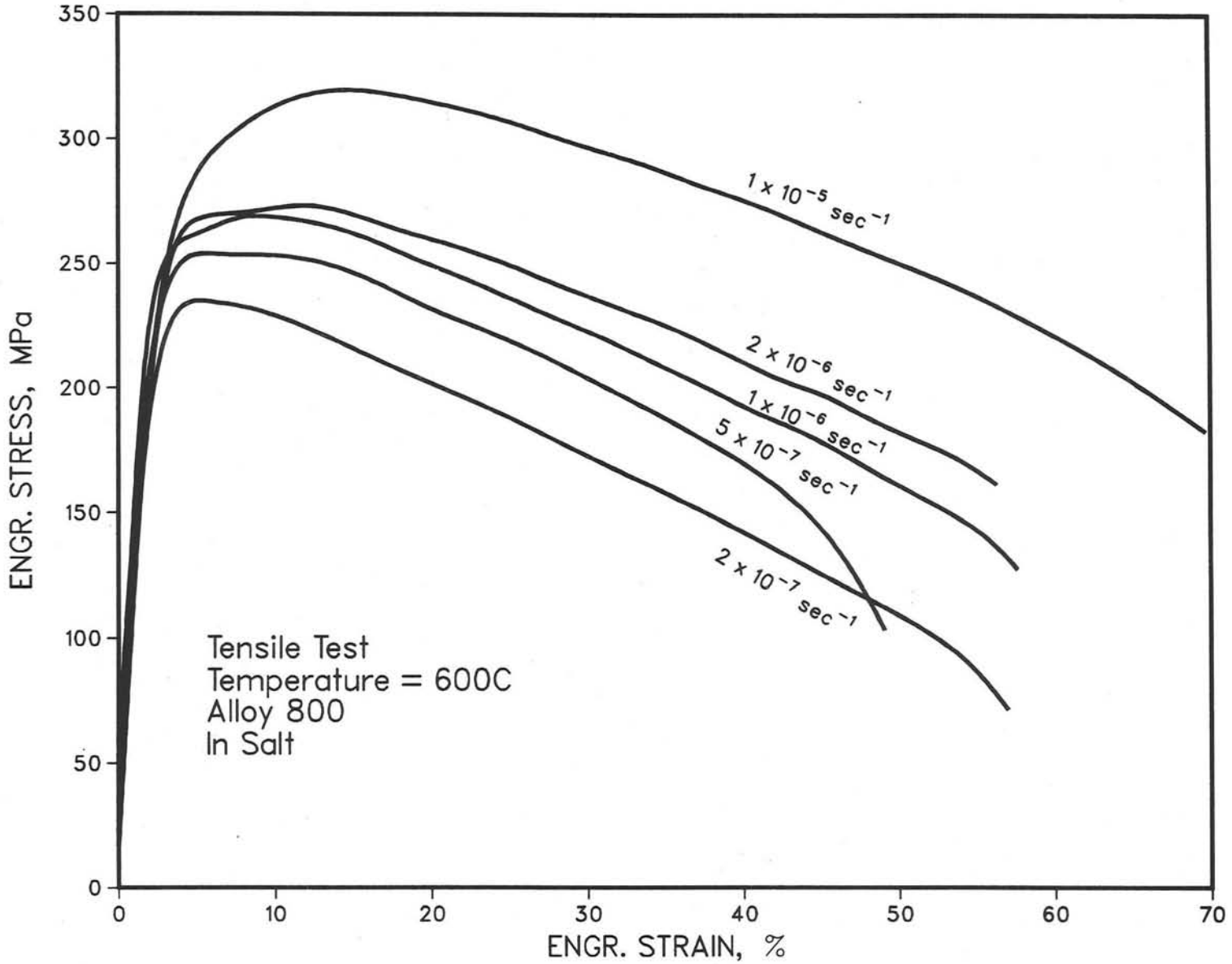

Figure 4. Stress-strain curves for Alloy 300 tested at 600°C is in the nitrate salt environment. The curves show the same general features as for those specimens tested in air.

Figure 5 compares directly the tensile curves for Alloy 800 at 600°C tested in salt (the solid curve) and in air (broken curve) at the same initial strain rate of 1×10^{-6} sec^{-1}. The curves virtually superimpose, thereby indicating the absence of any measurable environmental effect. The small difference in strain-to-fracture is clearly within the expected scatter for this quantity and not indicative of a change material behavior. The data for all the mechanical testing is summarized in Table 2. From this table it can be seen that there was no appreciable degradation in material behavior as the result of prolonged salt exposure. This is more clearly shown in Figure 6 which shows the influence of initial strain rate on total elongation (Figure 6a) and reduction in area (Figure 6b). Measured in this way, the ductility in both salt and air was comparable. As the strain rate was decreased the ductility of the salt exposed samples did not markedly decrease as would be expected if environmental or stress corrosion cracking was occurring.

The salt environment did not degrade the mechanical properties of Alloy 800 even though surface oxide scales formed rapidly. Figure 7 compares the deformed gage sections from two specimens, one tested in air and the other tested in salt at the same initial strain rate. The total environmental exposure times were thus nearly equivalent. The air exposed surface was free of surface oxides while the salt exposed surface exhibits an approximately 9μm thick surface scale. The intrusion of the oxide below the specimen surface visible in Figure 7b is the result of the extensive grain boundary cracking which occurs at the high imposed strains and slow strain rates. Although not apparent in Figure 7a, this cracking is ubiquitous, occurring at these temperatures and strains regardless of the environment. The cracking generally extends only one or two grain diameters below the surface and thus even though it allows the oxidizing environment to penetrate below the metal surface, it does not result in accelerated fracture.

Surface finish did not appear to plan an important role in either the kinetics of oxidation or in the resulting oxide morphology. Figure 8 compares the oxides formed on opposite sides of the deformed gage section of a single tensile specimen. In Figure 8a, the specimen surface was exposed to the salt in the as-machined condition while the oxide in Figure 8b was formed on a surface polished to a 600 grit finish. In both cases the oxides are equally thick and the oxide-base metal interfaces appear to be equivalent. This is contrary to the results of general corrosion (immersion) experiments (8) where the rate of oxide growth was found to be faster on rough surfaces than on polished surfaces. In addition, it had been found that the oxide-metal interface formed on the rough surfaces was considerably more irregular than the interface formed on a smooth surface. The discrepancy between current and previous findings may be simply one of degree. That is, the EDM surfaces may not be sufficiently different from the polished surfaces to yield a substantial effect either in growth rate or oxide-base metal interface morphology.

While the oxidizing environment does not result in a measurable ductility loss at the temperature and strain rates of these tests, deformation does affect the kinetics of oxidation and the oxide morphology. Figure 9 compares the oxide formed on the salt-exposed, deformed gage section to that formed on the exposed grip end which did not deform during the test. The oxide

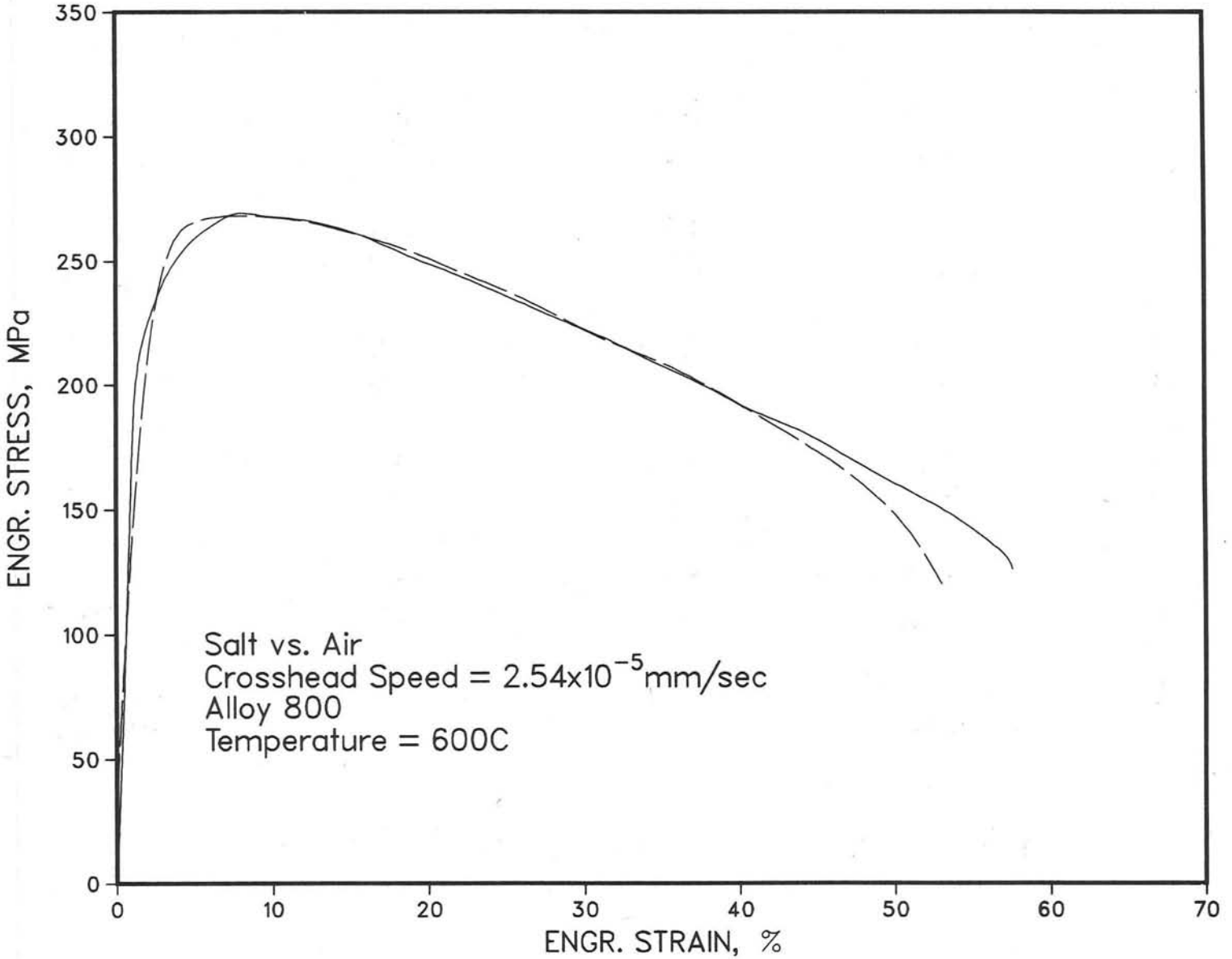

Figure 5. Comparison of two typical specimens, one tested in salt (solid curve), the other tested in air (broken curve). The superposition of the curves indicates the absence of any major environmental effect.

TABLE 2

TENSILE PROPERTIES OF 1800 AT 600°C

EXTENSION RATE(mm/sec)	CONDITION	UTS (MPa)	TOTAL ELONG. (%)	RA (%)
2.54×10^{-4}	Air	331	58.3	61.1
	Salt	319	68.7	53.5
5.08×10^{-5}	Air	284	58.9	63.1
	Salt	270	57.0	60.9
2.54×10^{-5}	Air	264	53.1	53.2
	Salt	266	58.9	52.7
1.27×10^{-5}	Air	253	53.2	53.3
	Salt	251	49.5	58.8
5.08×10^{-6}	Air	221	48.2	57.5
	Salt	223	56.9	45.0

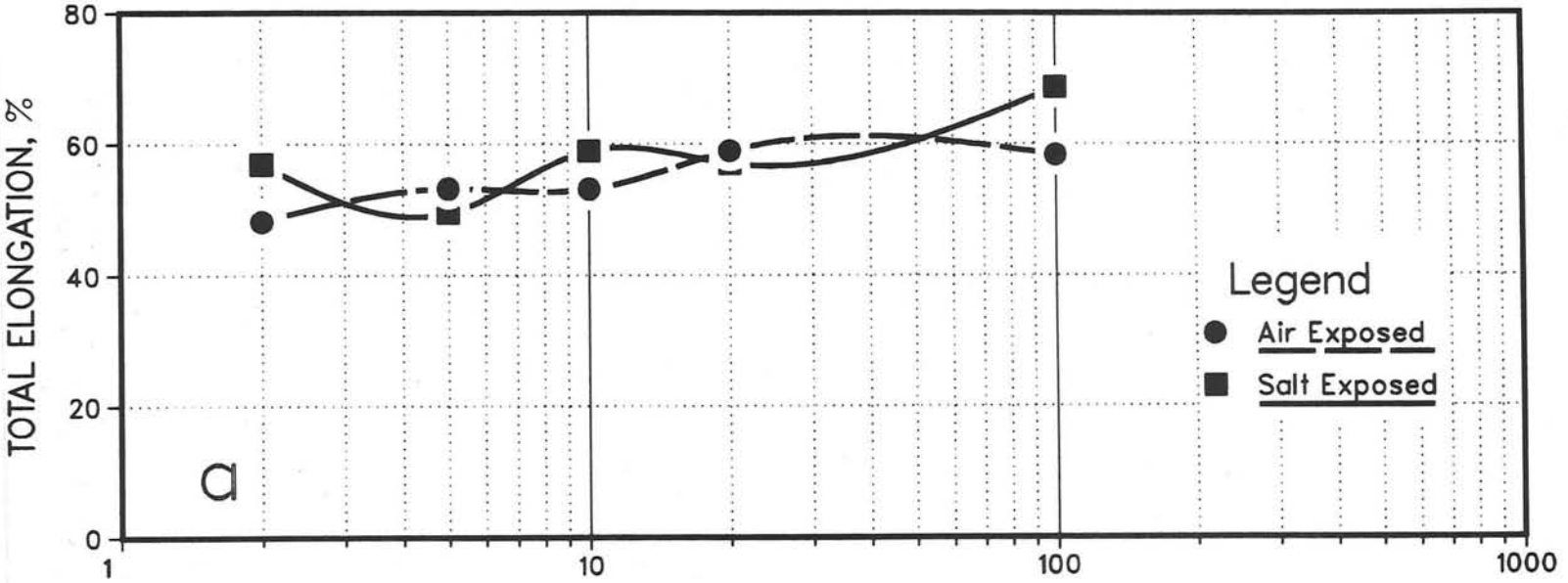

Figure 6a. Effect of strain rate on total elongation (strain to fracture) for Alloy 800.

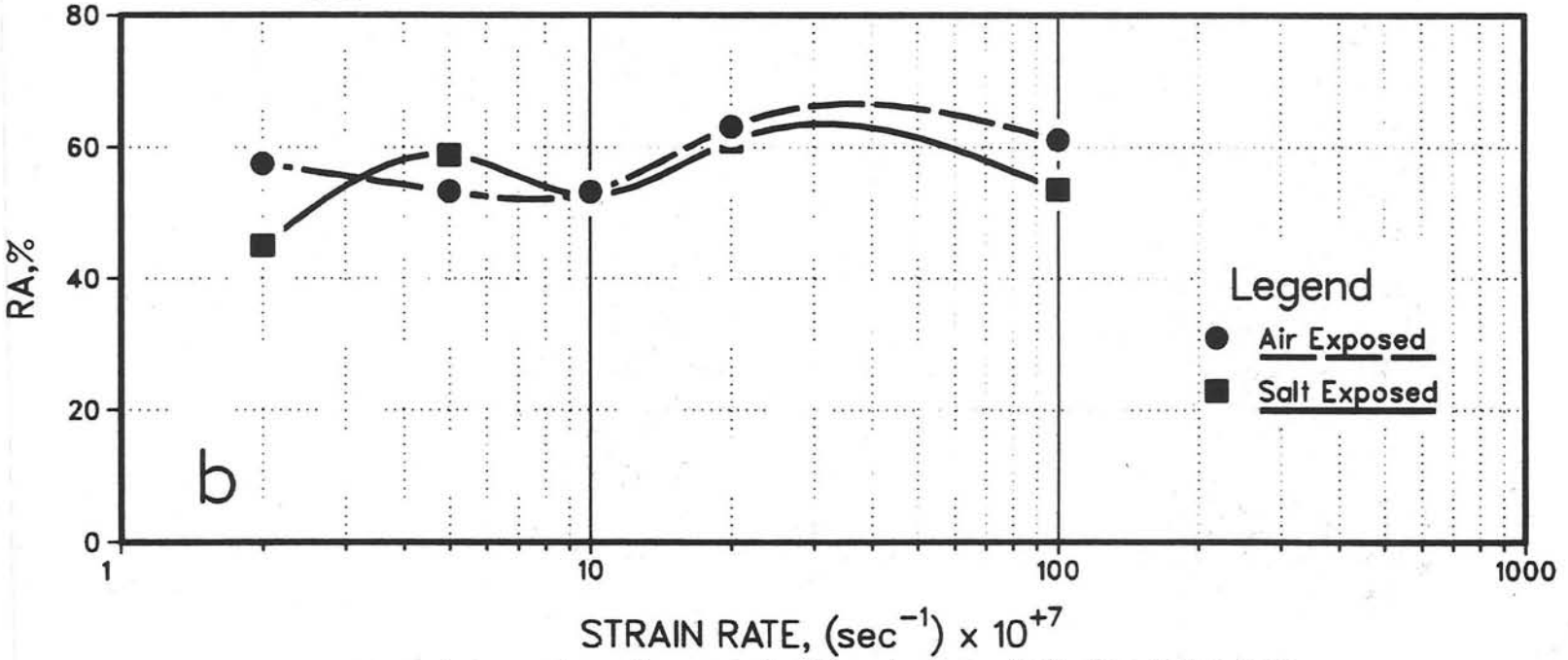

6b. Effect of strain rate on reduction in area (RA) for Alloy 800.

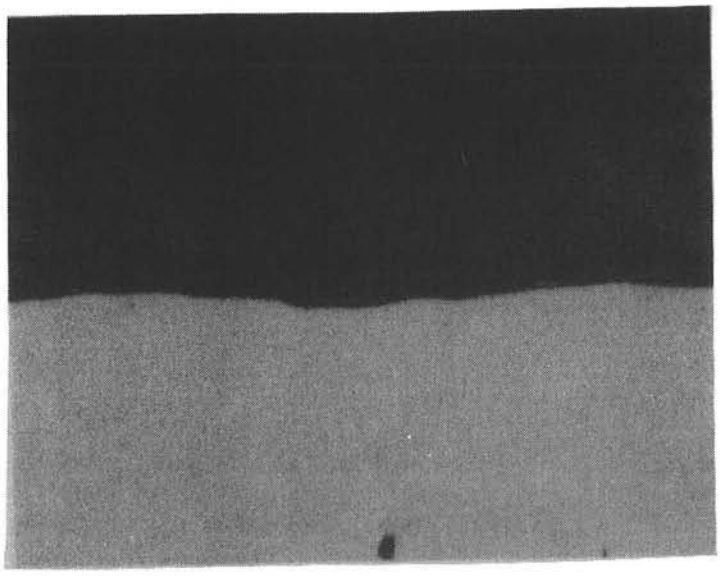

20 μm

a. Air Exposed (170 hours)

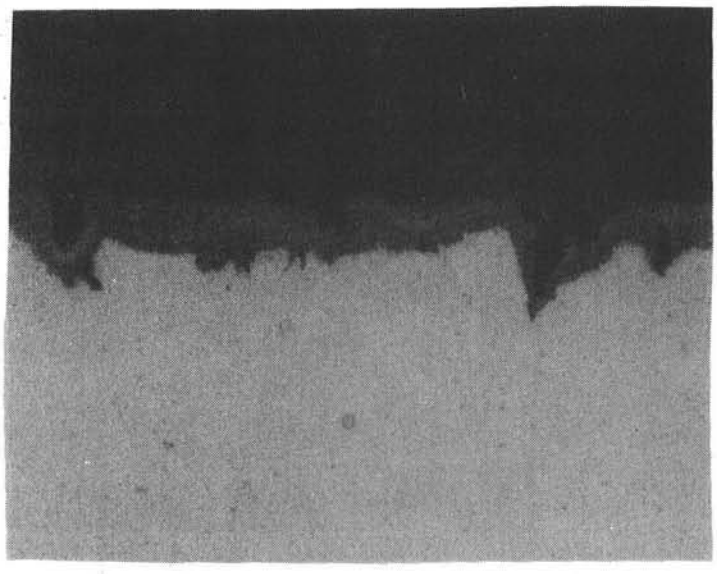

b. Salt Exposed (188 hours)

Figure 7. Comparison of air exposed, deformed gage section to a salt exposed, deformed gage section tested at the same initial strain rate and at 600°C. Total test time and therefore total time at temperature in the two environments are indicated in the parentheses (optical microscopy).

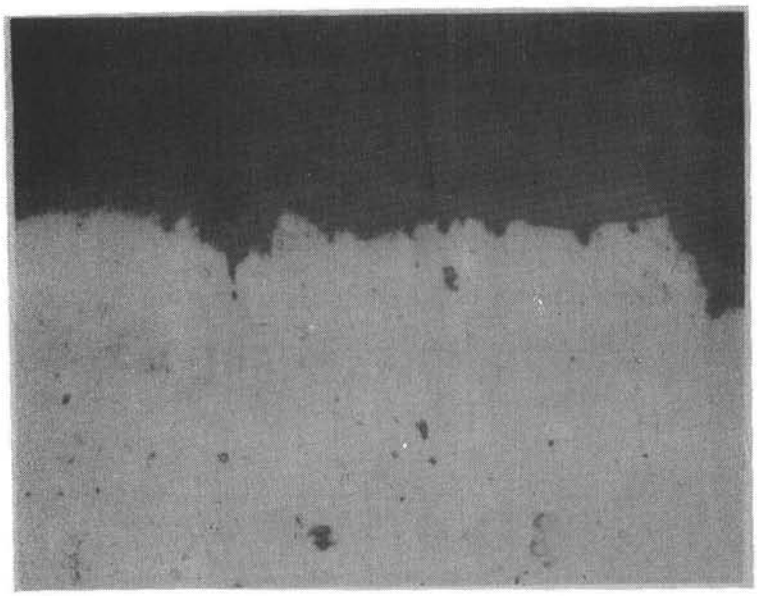

20 μm

a. As Machined (88 hours)

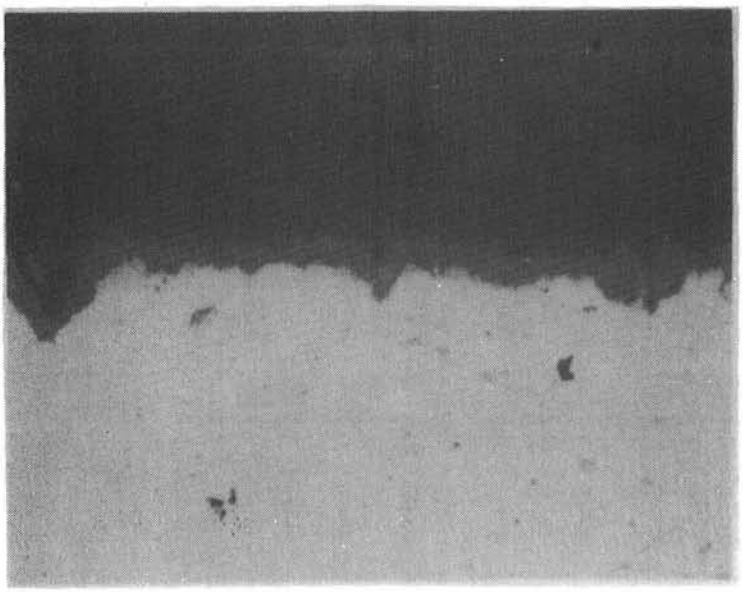

b. Polished (88 hours)

Figure 8. Effect of surface finish on oxide morphology. Both micrographs are taken from the opposite sides of the same gage section and therefore the total salt exposure times were the same. Surface finish had little effect on the structure of the oxide (optical microscopy).

Salt Exposed Surfaces
(960 hours)

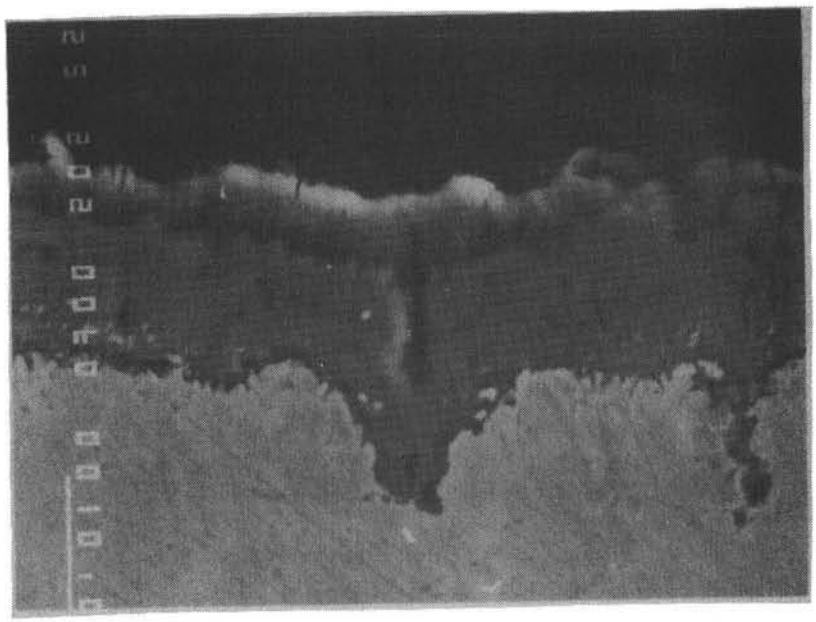

10 μm

a. Deformed Section

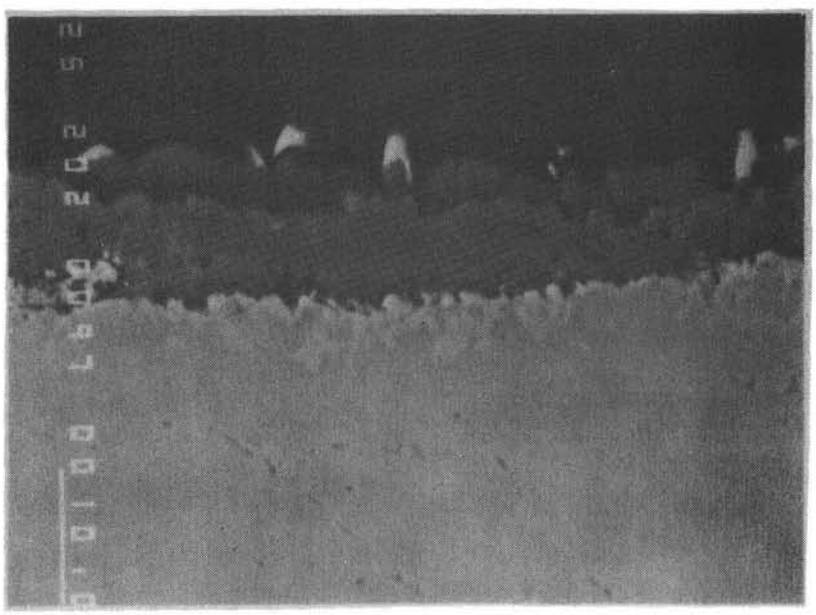

b. Undeformed Section

Figure 9. Effect of deformation on oxide thickness and morphology. Deformation increases the rate of oxide formation and results in a damaged surface scale (SEM).

film formed on the gage sections was ∿11μm in average thickness while the oxide formed on the undeformed surface section was only ∿70% as thick. In addition, the figure indicates that deformation results in more extensive microcracking of the surface scale than that present in the undeformed oxide. The oxide remains tenacious to the base metal. Flaking or spallation was not found to occur even at the high strains involved in the testing. The increased rate of oxidation on the deformed surfaces was observed at all strain rates for tests of all durations, as summarized in Figure 10. Note that in both cases the rate of oxide formation is rapid at first but then drops off dramatically with increased exposure time.

The evolution of the surface oxides formed on the alloy in the molten salt environment is shown in Figure 11. As stated above, surface scales form rapidly after short exposure times but the rate of formation decreases rapidly with increasing exposure times. Figure 11 indicates that for all exposure times, the oxide-base metal interface was generally well defined and uniform. Both the large and small intrusions of oxides into the alloy were the result of the extensive deformation-induced grain boundary cracking. The deepest intrusion observed was on the order of 40μm. This intrusion is small in extend compared to the specimen thickness of 1.27mm. The resulting loss of load bearing area resulting from this cracking never exceeded approximately 3% of the uniform cross-sectional area.

The surface oxides which form have a complex multiphase composition as evidenced by the multiple contrast features visible in the oxides shown in Figures 9 and 11. The multiphase regions within the oxides are apparent in the micrographs taken from the specimens exposed for short times (Figure 11d, e) as well as within the oxides formed on those specimens exposed for the longest times. Figure 12 illustrates the complexity of the oxide and near-oxide interface region of the base metal obtained via EDX analysis of the region corresponding to the electron image shown in Figure 12a. The near-surface oxide was found to be iron-rich and iron-poor. Nickel appears to be relatively immobile at this temperature, not occurring in the oxide at any significant concentration. The exact stiochiometry of the oxide phases is dependent on both the exposure temperature and exposure time.

CONCLUSIONS

The results of the mechanical testing in molten salt did not reveal an environmentally-induced degradation in structural properties. Strain to fracture, reduction in area and ultimate strength were not appreciably affected by exposure of Alloy 800 to the nitrate environment. Deformation resulted in the cracking of the surface oxide and acceleration of the oxide growth rate. That acceleration, while measurable, was not significant enough to affect the mechanical properties of the alloy measured in the SSRT experiments. Deformation did not affect the oxidation mode, that is, it remained one of relatively uniform surface attack. None of the microstructural evidenced revealed a propensity for environmental cracking to occur. The observed intrusions of the oxide into the base metal were the result of deformation-induced grain boundary cracking and <u>not</u> the result of exposure to the molten salt.

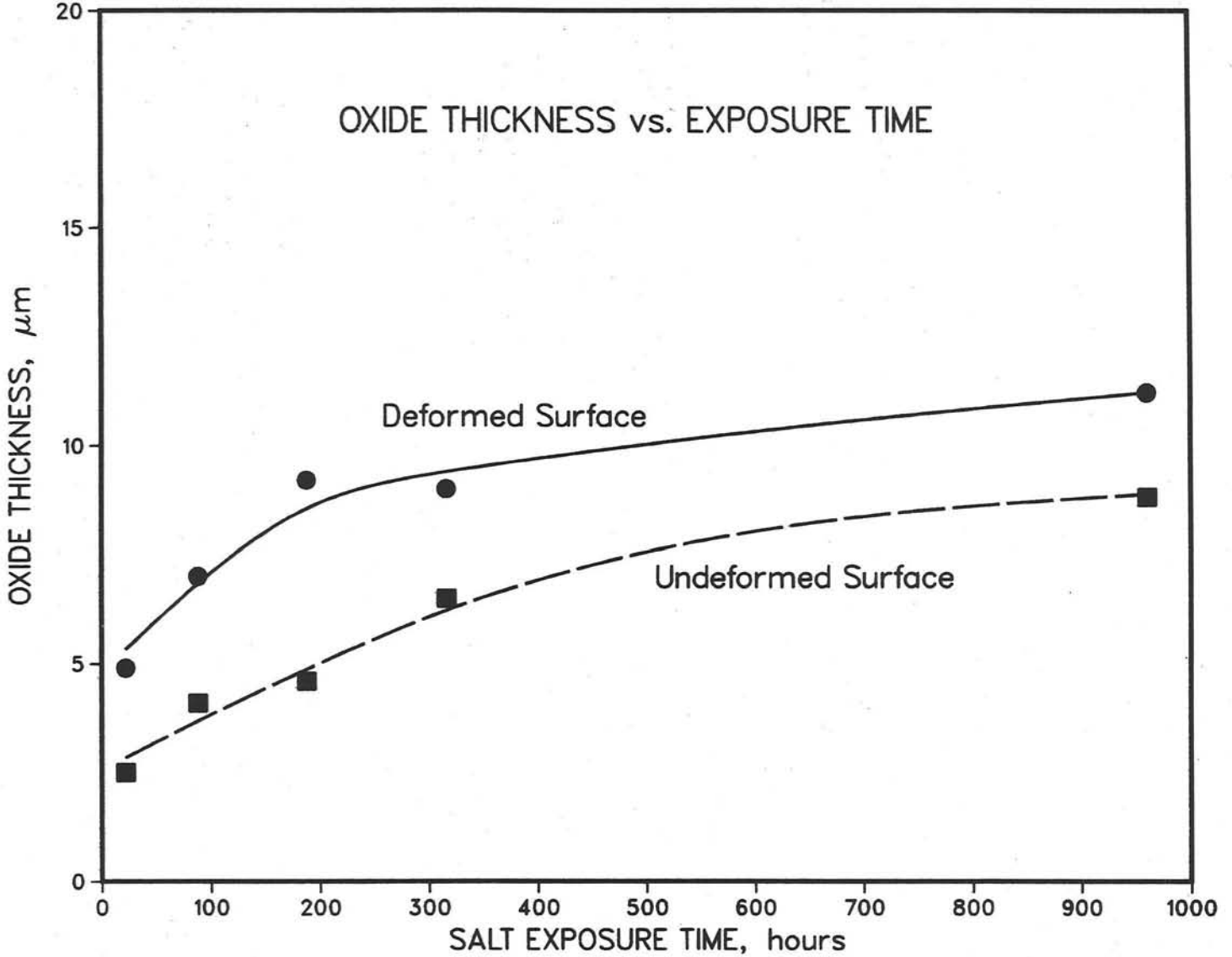

Figure 10. Effect of deformation on oxide thickness as a function of salt exposure time. For the testing performed, deformation results in an oxide which is uniformly thicker than those formed on the undeformed surfaces.

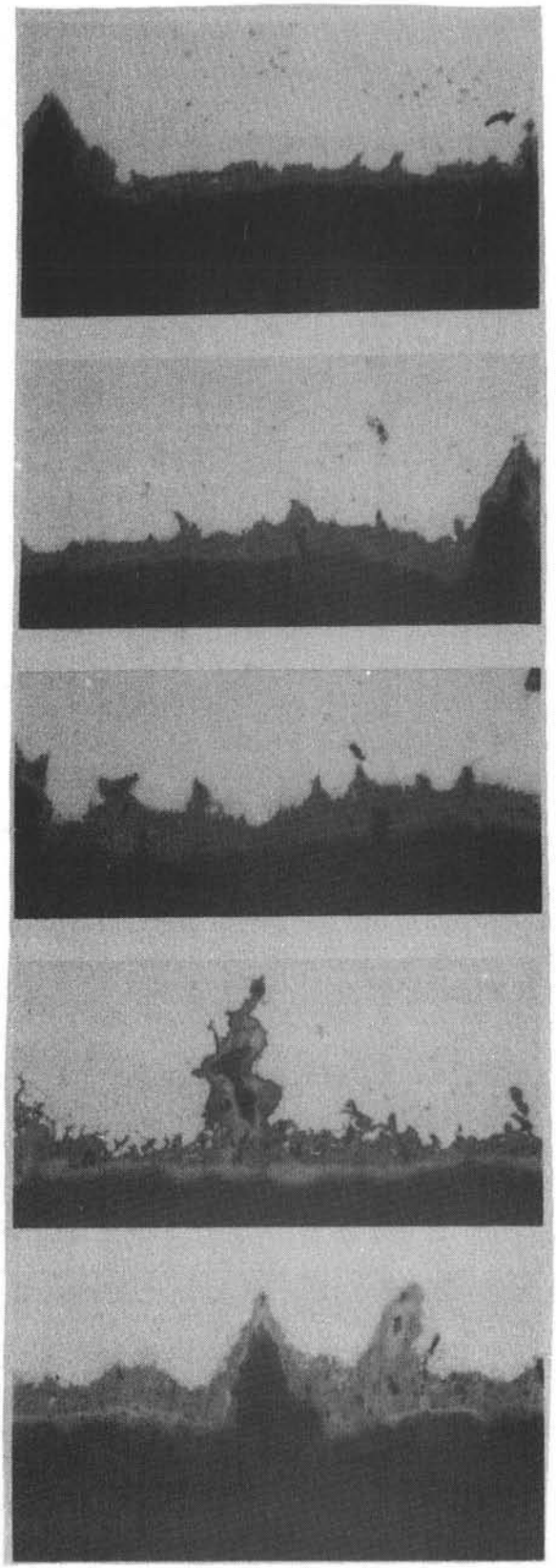

Salt Exposed Gage Sections

20 μm

a. 960 hours

b. 316 hours

c. 188 hours

d. 88 hours

e. 22 hours

Figure 11. Evolution of oxide scales for all SSRT specimens. Intrusion of the oxides within the base metal was the result of the extensive grain boundary cracking which occurred at the high strain levels imposed on the specimens (optical microscopy).

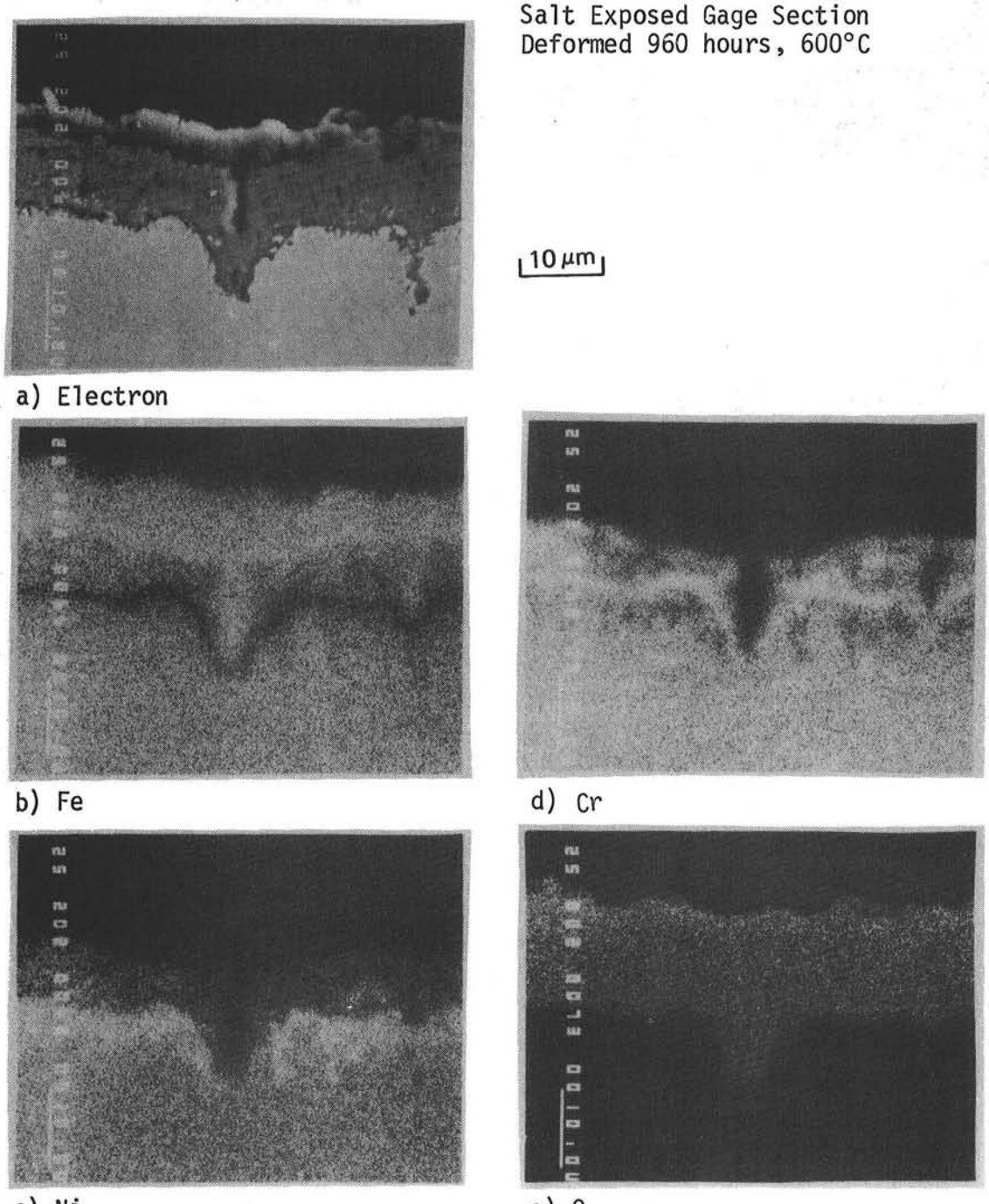

Figure 12. EDX characterization of the surface oxide formed after exposure to the molten salt for 960 hours at 600°C. Fe and Cr preferentially segregate within the oxide while Ni concentrates within the near oxide base metal.

In summary, the results of this experimental program reveal that nitrate salts appear to be a good choice for use as a thermal storage or heat transfer fluid from a materials compatibility standpoint, in that:

1. Corrosion does occur, but it is not a significant problem at 600°C.

2. Mechanical properties as measured in SSRT experiments are not significantly affected by exposure of Alloy 800 to the salt environment.

REFERENCES

1. R. W. Mar and J. C. Swearengen, "Materials Issues in Solar Thermal Energy Systems", Solar Energy Materials 5, (1981) 37-53.

2. S. H. Goods, "Environmental Compatibility and Materials Issues for Solar Central Receivers" presented at Pacific N. W. Metals and Minerals Corp., May, 1980.

3. D. A. Nissen, "Thermophysical Properties of the Equimolar Mixture $NaNO_3$-KNO_3 from 300-600°C" SAND80-8040.

4. R. W. Carling, Proceedings 3rd International Symposium on Molten Salts, Electrochem. Soc. Pennington, NJ, 1980, pp. 485.

5. C. M. Kramer, PhD Thesis, U.C. Davis, 1980.

6. "Stress Corrosion Cracking-The Slow Strain Rate Technique", G. M. Ugiansky and J. H. Payer Eds. ASTM STP 665, 1979.

7. S. H. Goods, "Creep and the Corrosion Characteristics of Incoloy Alloy 800 in Molten Nitrate Salts", SAND81-8665.

8. R. W. Bradshaw, Private Communication.

UNLIMITED RELEASE

INITIAL DISTRIBUTION

USDOE (3)
Division of Thermal and Mechanical Energy Storage Systems
MS 6B025 Room IG-100
Forrestal Building
Washington, D.C. 02585
Attn: J. H. Swisher
S. Strauch
M. Gurevich

USDOE
Albuquerque Operations Office
Special Programs Division
P.O. Box 5400
Albuquerque, NM 87115
Attn: D. Schueler

USDOE
San Francisco Operations Office
1333 Broadway
Oakland, CA 94612
Attn: D. Elliott

USDOE (5)
Division of Solar Thermal Energy Systems
600 E. Street N.W.
Room 419
Washington, D. C. 20585
Attn: G. W. Braun
M. U. Gutstein
J. E. Rannels
W. Auer
K. Cherian
W. Hochheiser

Aerospace Corporation (2)
2350 El Segundo Blvd.
El Segundo, CA 90009
Attn: P. Mathur
L. R. Stiney

J. H. DeVan
Oak Ridge National Laboratory
Oak Ridge, TN 37830

JPL (3)
4800 Oak Grove Dr.
Pasadena, CA 91103
Attn: V. Truscello
R. Manvi
J. Becker

EPRI (2)
P. O. Box 10412
3412 Hillview Ave.
Palo Alto, CA 94303
Attn: J. Bigger
T. R. Schneider

SERI (7)
1536 Cole Blvd.
Golden, CO 80401
Attn: B. Butler
B. P. Gupta
C. Wyman
P. A. Roberts
P. Russell
R. G. Nix
R. Ortiz (SERI Library)

Rockwell International
8900 De Soto Avenue
Canoga Park, CA 91304
Attn: Anarg Z. Frangos

Olin Corporation (3)
275 Winchester Ave.
New Haven, CT 06511
Attn: Louis C. Fiorucci
Stephen L. Goldstein
Joe K. Mensah

Olin Corporation (3)
120 Long Ridge Road
Stamford, CT 06904
Attn: Norman Christopher
Gerald A. Habib
Robert E. Smith

McDonnell Douglas (3)
5301 Bolsa Ave.
Huntington Beach, CA 92647
Attn: George F. Greenwalt
Donald L. Endicott
Russell T. Neher

Skip Gross
MSA Research
Evans City, PA 16033

Martin Marietta Corporation
Box 179
Denver, CO 80201
Attn: Tom Tracy

George H. Rowe
Combustion Engineering
1000 Prospect Hill Road
Windsor, CT 06095

Pacific Gas and Electric
3400 Crow Canyon Road
San Ramon, CA 94583
Attn: Helena T. Rowland

Stuart A. Shiels
Westinghouse Electric Corporate
Advanced Reactors Division
Box 158
Madison, PA 15663

Soeren S. Nielsen
Gould, Inc.
Rolling Meadows, IL 60008

Donald J. Liffengran
Stearns-Roger
4500 S. Cherry Creek Drive
Denver, CO 80217

James P. Maddox
Biphase Energy Systems
2800 Airport Avenue
Santa Monica, CA 90405

United Engineers and Construction
30 S. 17th Street
Philadelphia, PA 19103
Attn: John B. Mulligan

T. V. Narayanan
Foster Wheeler
12 Peach Tree Hill Road
Livingston, NJ 07039

Steve P. Harnden
Arizona Public Service Company
P.O. Box 21666
Phoenix, AZ 85036

Rockwell International/ETEC (2)
8900 De Soto Avenue
Canoga Park, CA 91304
Attn: Rich L. Howerton
Jerry B. Brukiewa

Rockwell International/ESG
8900 De Soto Avenue
Canoga Park, CA 91304
Attn: Ted Johnson

Robert L. Lessley
Bechtel
50 Beale
San Francisco, CA 94119

Robert J. Walter
Rocketdyne
6633 Canoga Avenue
Canoga Park, CA 91360

Sydney H. White
EIC Labs., Inc.
55 Chapel Street
Newton, MA 02158

Fred F. Witt
General Electric
3172 Porter Drive
Palo Alto, CA 94304

Donald J. Spellman
Gas Cooled Reactor Assoc.
3344 N. Torrey Pines Road
La Jolla, CA 92137

Pierra Spiteri
EDF
Les Renaidierz
Eculles
France

General Atomic Co. (2)
P.O. Box 81608
San Diego, CA 92138
Attn: Thomas H. Van Hagan
Daniel L. Vrable

George Yenetchi
Solar Thermal Systems
Division of Exxon Enterprises Inc.
P.O. Box 592
Florham Park, NJ 07932

Prof. Harald A. Oye
Institutt for uorganisk kjemi
Norges tekniski hogskole
N-7034 Trondheim - NTH, Norway

C. A. Bolthrunis
Badger Energy, Inc.
One Broadway
Cambridge, MA 02142

T. B. Cook, 8000; Attn: D. M. Olson, 8100
A. N. Blackwell, 8200
L. Gutierrez, 8400
B. F. Murphey, 8300
D. M. Schuster, 8310
D. A. Nissen, 8312
R. W. Mar, 8313
A. J. West, 8314
L. A. West, 8315
J. C. Swearengen, 8316
S. H. Goods, 8316 (10)
R. L. Rinne, 8320
G. W. Look, 8328
R. A. Baroody, 8410
R. C. Wayne, 8430
P. J. Eicker, 8431
L. G. Radosevich, 8431
R. W. Carling, 8431
C. S. Selvage, 8450
C. T. Yokomizo, 8451
A. C. Skinrood, 8452
W. G. Wilson, 8453
D. B. Dawson, 8453
C. M. Tapp, 8460
D. L. Hartley, 8500
Publications Division, 8265, for TIC (2)
Publications Division, 8265/Technical Library Processes Division, 3141
Technical Library Processes Division, 3141 (3)
M. A. Pound, 8214, for Central Technical Files (3)